



Reversible Dehydration in Polyoxometalate-Based Hybrid Compounds: A Study of Single-Crystal to Single-Crystal Transformations in Keggin-Type Germanotungstates Decorated with Copper(II) Complexes of Tetradentate N-Donor Ligands

Amaia Iturrospe,[†] Leire San Felices,[‡] Santiago Reinoso,[†] Beñat Artetxe,[†] Luis Lezama,^{†,§} and Juan M. Gutiérrez-Zorrilla*,^{†,‡,§}

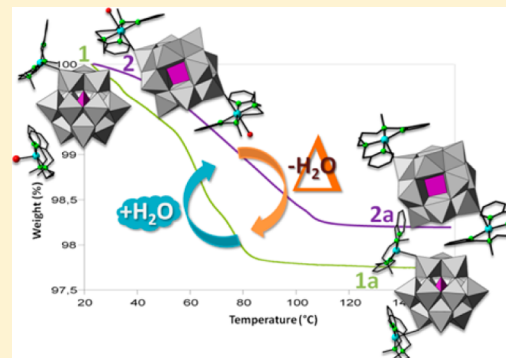
[†] Departamento de Química Inorgánica, Facultad de Ciencia y Tecnología, Universidad del País Vasco UPV/EHU, P.O. Box 644, 48080 Bilbao, Spain

[‡] Servicios Generales de Investigación (SGIker), Facultad de Ciencia y Tecnología, Universidad del País Vasco UPV/EHU, P.O. Box 644, 48080 Bilbao, Spain

[§] Basque Center for Materials, Applications & Nanostructures (BCMaterials), Parque Científico y Tecnológico de Bizkaia, Ibaizabal Bidea, Edificio 500 – Planta 1, 48160 Derio, Spain

Supporting Information

ABSTRACT: Hydrothermal reaction of the Keggin-type $[\alpha\text{-GeW}_{11}\text{O}_{39}]^{8-}$ anion with copper(II) complexes of the tetradentate N-donor ligands *N,N'*-dimethyl-*N,N'*-bis-(pyridine-2-ylmethyl)-1,2-diaminoethane (bpmen) or *N,N'*-dimethyl-*N,N'*-bis-(pyridine-2-ylmethyl)-1,3-diaminopropane (bpmpn) results in three new hybrid compounds $[\text{Cu}(\text{bpmen})(\text{H}_2\text{O})]\cdot[\text{GeW}_{12}\text{O}_{40}\{\text{Cu}(\text{bpmen})\}]\cdot3\text{H}_2\text{O}$ (**1**), $[\text{GeW}_{12}\text{O}_{40}\{\text{Cu}(\text{bpmpn})(\text{H}_2\text{O})\}_2]\cdot3\text{H}_2\text{O}$ (**2**), and $[\text{Cu}(\text{bpmpn})(\text{H}_2\text{O})][\text{GeW}_{12}\text{O}_{40}\{\text{Cu}(\text{bpmpn})\}]\cdot8\text{H}_2\text{O}$ (**3**). All compounds have been characterized by elemental analyses and infrared spectroscopy, and their structures have been established by single-crystal X-ray diffraction. Both **1** and **3** contain monodecorated polyanions and additional complex cations, but their layered structures show noticeable differences. For **1**, the polyanions are arranged in rows whose stacking generates intralamellar cavities where complex cations and lattice water molecules are hosted, whereas double-layers of hybrid anions pillared by the cations occupying the interlamellar space are observed for **3**. In the case of **2**, the packing of trans-didecorated clusters generates honeycomb-like metalorganic layers and perpendicular hexagonal channels where Keggin moieties are nested. A combination of thermogravimetric and variable temperature powder X-ray diffraction analyses show that dehydration of **1** and **2** results in thermally stable, crystalline phases. Dehydrations are fully reversible upon exposure to air and proceed via single-crystal to single-crystal transformations implying rupture/formation processes in the copper(II) bonding and consequent geometrical and conformational modifications in the complexes. Transformations have been followed by single-crystal X-ray diffraction, allowing for the structures of the anhydrous phases $[\text{GeW}_{12}\text{O}_{40}\{\text{Cu}(\text{bpmen})\}_2]$ (**1a**) and $[\text{GeW}_{12}\text{O}_{40}\{\text{Cu}(\text{bpmpn})\}_2]$ (**2a**) to be determined. Dehydration of **1** into **1a** with consequent formation of neutral, didecorated clusters does not result in the collapse of the intralamellar cavities but rather in an open-framework structure with slit-shaped micropores. Structural variations between **1** and **2** and their corresponding anhydrous phases are reflected in the electron paramagnetic resonance spectra.



INTRODUCTION

Polyoxometalates (POMs) form a remarkable family of versatile metal–oxygen clusters with controllable size, shape, composition, charge density, solubility, redox potential, and acid strength. These features make POMs potentially useful in a number of scientific areas related to topics of current technological interest, including catalysis, magnetism, materials science, or medicine.¹ The construction of POM-based hybrid compounds upon combination with transition-metal coordination complexes bearing organic ligands is in the current forefront of synthetic POM chemistry.² Functionalization of

POM clusters provides a promising route to merge the inherent properties of inorganic and metalorganic components synergistically, thus creating hybrid compounds with novel structures, properties, and/or applications.³

Tens of POM-based inorganic-metalorganic hybrid compounds have been reported in the last two decades, and among them, a large number have been prepared by using simple,

Received: January 7, 2014

Revised: March 14, 2014

Published: March 19, 2014



Table 1. Crystallographic Data for Compounds 1, 2, and 3 and the Anhydrous Phases 1a and 2a

	1	1a	2	2a	3
formula	C ₃₂ H ₅₃ Cu ₂ N ₈ O _{44.5} GeW ₁₂	C ₃₂ H ₄₄ Cu ₂ N ₈ O ₄₀ GeW ₁₂	C ₃₄ H ₅₈ Cu ₂ N ₈ O ₄₅ GeW ₁₂	C ₃₄ H ₄₈ Cu ₂ N ₈ O ₄₀ GeW ₁₂	C ₃₄ H ₆₆ Cu ₂ N ₈ O ₄₉ GeW ₁₂
fw (g mol ⁻¹)	3667.69	3586.53	3704.66	3614.67	3776.82
cryst syst	monoclinic	monoclinic	monoclinic	monoclinic	triclinic
space group	P2 ₁ /c	P2 ₁ /n	P2 ₁ /n	P2 ₁ /n	P1̄
T (K)	100(2)	423(2)	100(2)	423(2)	100(2)
a (Å)	11.5427(1)	11.4677(1)	11.0268(3)	10.8619(2)	12.7695(2)
b (Å)	22.4140(1)	22.5699(3)	12.1249(3)	11.9467(2)	13.0603(3)
c (Å)	25.8492(2)	25.3959(3)	24.7245(6)	24.0621(5)	21.2588(5)
α (deg)	90	90	90	90	79.433(2)
β (deg)	102.449(1)	102.372(1)	96.305(2)	97.937(2)	78.032(2)
γ (deg)	90	90	90	90	76.043(2)
V (Å ³)	6530.4(1)	6420.4(2)	3285.6(1)	3092.5(1)	3332.6(1)
Z	4	4	2	2	2
D _{calcd} (g cm ⁻³)	3.730	3.710	3.745	3.882	3.764
μ (mm ⁻¹)	39.970	22.602	22.095	42.126	39.256
collected reflns	53179	43638	22415	11512	23425
unique reflns (R _{int})	12121 (0.066)	11313 (0.058)	6460 (0.038)	5505 (0.036)	11880 (0.047)
observed reflns [I > 2σ(I)]	11844	8503	5916	5066	9565
params	485	423	334	317	436
R(F) ^a [I > 2σ(I)]	0.055	0.044	0.043	0.060	0.070
wR(F ²) ^a (all data)	0.146	0.106	0.086	0.132	0.220
GOF	1.132	1.060	1.218	1.174	1.025

^a(F) = Σ||F_o - F_c||/Σ|F_o|. wR(F²) = {Σ[w(F_o² - F_c²)²]/Σ[w(F_o²)²]}^{1/2}.

commercial organic ligands of bidentate character (e.g., diamines, bipyridines, oxalate).⁴ The intrinsic interest of these studies relies mainly on the search for new synthetic and architectural paradigms, but the report of relevant properties beyond is still scarce for this type of compounds. The use of more elaborate ligands might help to narrow this gap, bringing POM-based hybrids to new levels.

In that sense, we recently reported the fully reversible desorption/resorption of water associated with two compounds based on the Keggin-type [SiW₁₂O₄₀]⁴⁻ anion and copper(II) complexes of tetradentate ligands containing amine and pyridil groups (N₂Py₂),⁵ a type of ligand that has been successfully applied in catalytic and biomedical studies.⁶ Some other examples of POM-based compounds with reversible water sorption ability can be found in the literature, and these mainly include different types of porous materials with open-framework structures (from purely inorganic assemblies to ionic POM-(metal)organic hybrid crystals).⁷ In contrast, our compounds show compact, layered structures with water molecules either coordinated to metal atoms or residing in interstitial spaces.

Interestingly, the water desorption/resorption process in compounds [SiW₁₂O₄₀]⁴⁻/Cu(N₂Py₂) takes place upon heating via single-crystal to single-crystal (SCSC) transformations that are facilitated by cooperative POM-ligand interactions and imply rupture/formation of bonds around the Cu^{II} centers. Such type of solid-state phase transitions as a result of external stimuli (e.g., temperature, pressure, light, redox agents, guests) is a current focus of attention in crystal engineering,⁸ but reports on SCSC transformations in POM structures are rare.⁹ To our knowledge, only two other temperature-dependent processes have been described, both involving room- and low-temperature polymorphs.¹⁰

To determine whether the reported SCSC behavior constitutes a common feature in POM architectures derived

from N₂Py₂ ligands or represents just a serendipitous finding, we decided to extend our studies to related POM-based hybrids. We were first interested in exploring the structural influence of the POM cluster, and more specifically, the role of the central heteroatom in Keggin-type building-blocks. It has been shown that the construction of inorganic–metalorganic hybrids based on Keggin POMs is influenced by the heteroatom¹¹ because the physicochemical properties of the [XM₁₂O₄₀]ⁿ⁻ clusters depend to a great extent on the nature of X (size, charge, electronegativity) for a given addenda metal. For example, the acid/base properties of Keggin POMs are directly related to the electronegativity of X, in such a way that the cluster becomes less basic (less nucleophilic) as the electronegativity of X increases. The heteroatomic effect has been thoroughly studied for years, showing that properties undergo remarkable changes for heteroatoms in the same row, whereas variations are more subtle for heteroatoms in the same group.¹²

Here, we report the synthesis, thermal behavior, and crystal structures of three new hybrid compounds obtained from the interaction between the Keggin-type [GeW₁₂O₄₀]⁴⁻ anion and Cu^{II}/N₂Py₂ complexes of the bpmen and bpmpn ligands: [Cu(bpmen)(H₂O)][GeW₁₂O₄₀{Cu(bpmen)}][·]3H₂O (**1**), [GeW₁₂O₄₀{Cu(bpmpn)(H₂O)}][·]3H₂O (**2**), and [Cu(bpmpn)(H₂O)][GeW₁₂O₄₀{Cu(bpmpn)}][·]8H₂O (**3**). Compounds **1** and **2** undergo thermally induced dehydration processes that are fully reversible upon exposure to air and proceed via SCSC transformations. The structures of the anhydrous phases [GeW₁₂O₄₀{Cu(bpmen)}]₂ (**1a**) and [GeW₁₂O₄₀{Cu(bpmpn)}]₂ (**2a**) have also been determined by single-crystal X-ray diffraction. Among all compounds, the pair formed by **2** and **2a** is the only one isostructural with the previous silicon analogues.

EXPERIMENTAL SECTION

Materials and Methods. The $K_8[\alpha\text{-GeW}_{11}\text{O}_{39}] \cdot 13\text{H}_2\text{O}$ precursor was synthesized following literature methods¹³ and identified by infrared (FT-IR) spectroscopy. The ligands bpmen and bpmpn were prepared as described in our previous work⁵ and identified by ¹H nuclear magnetic resonance (NMR) spectroscopy. All other chemicals were obtained from commercial sources and used without further purification. Carbon, hydrogen, and nitrogen were determined on a Perkin-Elmer 2400 CHN analyzer. ¹H NMR spectra were recorded on a Bruker AC-300 spectrometer. FT-IR spectra (Figure S1 in the Supporting Information) were obtained as KBr pellets on a SHIMADZU FTIR-8400S spectrometer. Thermogravimetric and differential thermal analyses (TGA/DTA) were carried out from room temperature to 750 °C at a rate of 5 °C min⁻¹ on a TA Instruments 2960 SDT thermobalance under a 100 cm³·min⁻¹ flow of synthetic air. Powder X-ray diffraction (PXRD) patterns were collected from 30 to 890 °C every 20 °C on a Bruker D8 Advance diffractometer with 2θ steps of 0.033° in the 5 ≤ 2θ ≤ 39° range. Electron paramagnetic resonance (EPR) spectra were recorded on Bruker ELEXSYS 500 (superhigh-Q resonator ER-4123-SHQ) and Bruker EMX (ER-510-QT resonator) continuous wave spectrometers for Q- and X-bands, respectively (magnetic calibration: NMR probe; frequency inside the cavity determined with microwave counter).

Synthetic Procedure. A mixture of $K_8[\alpha\text{-GeW}_{11}\text{O}_{39}] \cdot 13\text{H}_2\text{O}$ (0.322 g, 0.10 mmol), $\text{Cu}(\text{CH}_3\text{CO}_2)_2$ (0.036 g, 0.30 mmol), $N_2\text{Py}_2$ ligand (0.20 mmol), and $\text{KCH}_3\text{CO}_2/\text{CH}_3\text{CO}_2\text{H}$ 1 M buffer solution (25 mL) was stirred for 1 h, transferred to a 50 mL Teflon-lined autoclave, and kept at 140 °C for 72 h. Compounds 1–3 were isolated as single crystals suitable for X-ray diffraction after cooling the reaction mixture to room temperature for 48 h.

[Cu(bpmen)(H₂O)][GeW₁₂O₄₀{Cu(bpmen)}]·3.5H₂O (1). The ligand bpmen (0.054 g, 0.20 mmol) was used, and 99 mg of 1 was isolated as blue plates (yield: 27% based on W). Anal. calcd (found) for $C_{32}\text{H}_{53}\text{Cu}_2\text{N}_8\text{O}_{44.5}\text{GeW}_{12}$: C, 10.48 (10.55); H, 1.46 (1.31); N, 3.06 (3.10). IR (cm⁻¹): 3084(w), 2928(w), 1611(m), 1446(m), 1306(w), 1258(w), 1030(w), 966(s), 880(s), 831(s), 785(s), 756(s), 520(m), 463(m).

[GeW₁₂O₄₀{Cu(bpmpn)}]·3H₂O (2) and [Cu(bpmpn)(H₂O)][GeW₁₂O₄₀{Cu(bpmpn)}]·8H₂O (3). The ligand bpmpn (0.057 g, 0.20 mmol) was used, and a mixture of orange hexagonal plates of 2 as the major fraction and blue plates of 3 as a side-product was obtained. Crystals of each compound were manually separated under an optical microscope for full characterization and structural determination.

Compound 2. Yield: 92 mg, 25% based on W. Anal. Calcd (found) for $C_{34}\text{H}_{58}\text{Cu}_2\text{N}_8\text{O}_{45}\text{GeW}_{12}$: C, 11.02 (10.98); H, 1.58 (1.63); N, 3.02 (3.09). IR (cm⁻¹): 3117(w), 2924(w), 1611(m), 1476(m), 1443(m), 1296(w), 1030(w), 966(s), 881(s), 829(s), 785(s), 538(m), 463(m).

Compound 3. Yield: lower than 2% based on W. Anal. Calcd (found) for $C_{34}\text{H}_{66}\text{Cu}_2\text{N}_8\text{O}_{49}\text{GeW}_{12}$: C, 10.81 (10.72); H, 1.76 (1.86); N, 2.97 (3.11). IR (cm⁻¹): 2924(w), 1612(m), 1443(m), 1302(w), 1256(w), 968(s), 883(s), 829(s), 783(s), 540(m), 463(m).

X-ray Crystallography. Crystallographic data for 1, 2, and 3 and for the anhydrous phases 1a and 2a are given in Table 1. Intensity data were collected on an Agilent Technologies Super-Nova diffractometer, which was equipped with monochromated Cu $\text{K}\alpha$ radiation ($\lambda = 1.5418\text{\AA}$) and Atlas CCD detector in all cases with the exception of 1a and 2. For the latter, the selected radiation and detector were monochromated Mo $\text{K}\alpha$ ($\lambda = 0.71073\text{\AA}$) and Eos CCD, respectively. Measurements were carried out at 100(2) K for 1–3, and with the help of an Oxford Cryostream 700 PLUS temperature device, at 423(2) K for the anhydrous phases 1a and 2a. Data frames were processed (unit cell determination, analytical absorption correction with face indexing, intensity data integration and correction for Lorentz and polarization effects) using the CrysAlis software package.¹⁴ The structures were solved using OLEX¹⁵ and refined by full-matrix least-squares with SHELXL-97.¹⁶ Final geometrical calculations were carried out with Mercury¹⁷ and PLATON¹⁸ as integrated in WinGX.¹⁹

Thermal vibrations were treated anisotropically for heavy atoms (W, Cu, Ge). Hydrogen atoms of the organic ligands were placed in calculated positions and refined using a riding model with standard SHELXL parameters. For 2 and its anhydrous phase 2a, all the O atoms of the Keggin clusters were disordered in two positions each. All O pairs (e.g., O1A/O1B) were refined with the same population ratios, resulting in occupancies near 50% for all sites (49.6/50.4% in 2 and 48.1/51.9% in 2a).

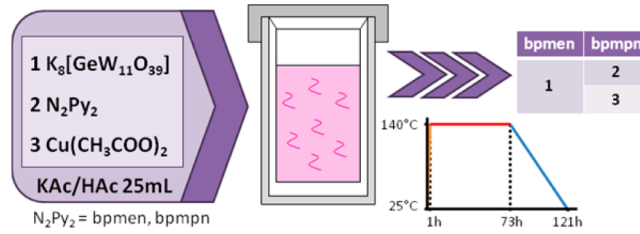
The complex acting as counterion in 3 also showed crystallographic disorder with three different Cu positions in the Fourier map (Cu1B, Cu1C, and Cu1D). The sum of the population factors of the three sites was restricted to 1, and the following occupancies were obtained: 37.7% for Cu1B, 44.2% for Cu1C, and 18.1% for Cu1D. The surrounding region of the Fourier map showed several maxima of low intensity at very short distances as a result of the overlapping of three bpmpn ligands associated to the Cu1B/C/D sites. This precluded discrimination of most of the C and N atomic positions, and hence we could only locate the $N_2\text{Py}_2$ backbone (without N-methyl groups) of the ligand corresponding to the Cu1B site. Up to 11 restraints in the interatomic distances were introduced to refine this organic fragment.

RESULTS AND DISCUSSION

Synthesis. Recently, we reported fully reversible desorption/readsoption of water via SCSC transformations in two hybrid compounds containing $[\alpha\text{-SiW}_{12}\text{O}_{40}]^{4-}$ anions and $\text{Cu}^{II}/N_2\text{Py}_2$ complexes upon heating and air-exposure.⁵ Following this work, we decided to undergo systematic crystallochemical studies on related POM-based hybrids to determine whether the reported behavior constitutes a common feature in this type of compounds or represents just a serendipitous yet interesting finding. As the first step, we replaced silicotungstates with other Keggin-type precursors (X = Ge^{IV}, P^V) in our syntheses to explore the influence of the heteroatom X in the structures.

Compounds 1–3 were obtained by hydrothermal treatment of a mixture of $K_8[\alpha\text{-GeW}_{11}\text{O}_{39}] \cdot 13\text{H}_2\text{O}$, $\text{Cu}(\text{CH}_3\text{CO}_2)_2$ and $N_2\text{Py}_2$ ligand (1:3:2 ratio) in a $\text{K}(\text{CH}_3\text{CO}_2)$ buffer (Scheme 1).

Scheme 1. Synthetic Approach for Compounds 1–3



Compound 1 is isolated as a single crystalline phase, whereas 2 and 3 are obtained as a mixture of crystals, the former representing the major phase and the latter a side product that is obtained in trace amounts. PXRD analyses confirm the homogeneity of the crystalline phases of 1 and 2 after manual separation (Figure S2 in the Supporting Information). Since 1–3 contain $[\alpha\text{-GeW}_{12}\text{O}_{40}]^{4-}$ plenary clusters instead of the monolacunary $[\alpha\text{-GeW}_{11}\text{O}_{39}]^{8-}$ precursor, we also tried to prepare these compounds following the procedure above but using $K_4[\alpha\text{-GeW}_{12}\text{O}_{40}]$ prepared as reported.¹³ These attempts resulted in light-brown (bpmen) and dark-brown (bpmpn) precipitates, which only in the case of the bpmpn ligand corresponded to pure 2 according to the PXRD patterns.

Variations in the size and charge of the POM heteroatom have a significant influence on the final products. Compounds containing monodecorated hybrid POMs and complex cations

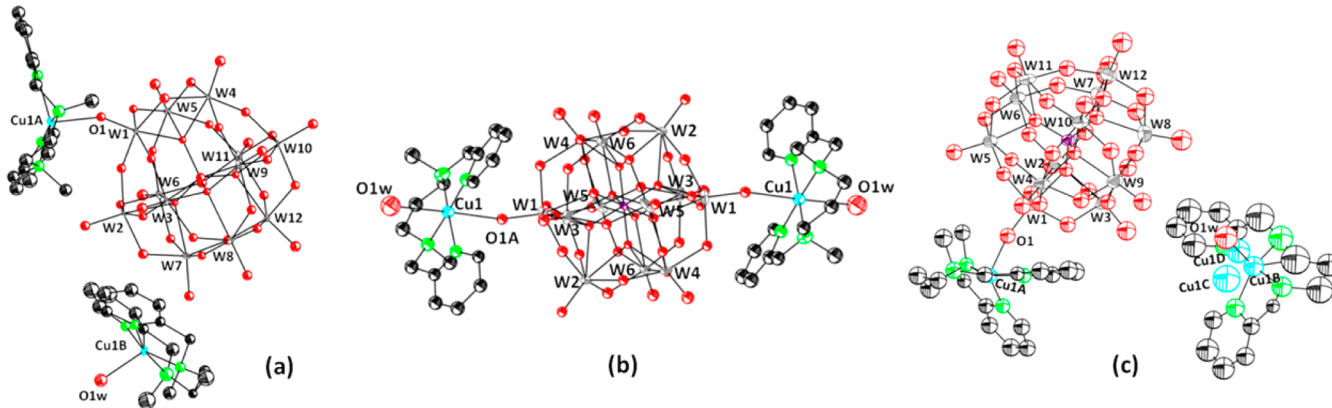


Figure 1. ORTEP view of the asymmetric units of (a) **1**, (b) **2**, and (c) **3** (50% displacement ellipsoids). Hydrogen atoms and lattice water molecules are omitted for clarity.

for the bpmen ligand and neutral didecorated species for the bpmpn ligand were isolated as single crystalline phases with the silicotungstate precursor.⁵ In the case of bpmen, the compound obtained when Si^{IV} is replaced with the larger Ge^{IV} (**1**) also contains monodecorated POMs and complex cations, but it consists of a hemiheptahydrate phase instead of the nonhydrate phase observed for Si^{IV}. Remarkable structural differences are derived from this higher degree of hydration, which are reflected not only in the less compact packing of **1** compared to the Si-analogue but also in its anhydrous **1a** derivative as explained below. For bpmpn, the use of Ge^{IV} instead of Si^{IV} did not result in a pure compound but rather in a mixture of crystals. Although the major phase (**2**) is isostructural with the Si-containing compound, the structure of the side product (**3**) does not contain didecorated species, being closely related to the bpmen derivatives. Reactions for both ligands were also carried out with the less charged $[\alpha\text{-PW}_{11}\text{O}_{39}]^{7-}$ precursor. Unfortunately, they did not result in any crystalline material but only in amorphous precipitates unsuitable for full characterization.

Crystal Structures. Compounds **1** and **2** crystallize in the monoclinic space group $P2_1/c$ and $P2_1/n$, respectively, whereas compound **3** crystallizes in the triclinic space group $P\bar{1}$. The asymmetric units of **1** and **3** contain one hybrid polyanion $[\text{GeW}_{12}\text{O}_{40}\{\text{Cu}(\text{N}_2\text{Py}_2)\}]^{2-}$ (N_2Py_2 : bpmen for **1** and bpmpn for **3**), one nonsupported $[\text{Cu}(\text{N}_2\text{Py}_2)(\text{H}_2\text{O})]^{2+}$ complex, and several water molecules of hydration. In contrast, the asymmetric unit of **2** is composed of a $[\text{GeW}_{12}\text{O}_{40}\{\text{Cu}(\text{bpmpn})(\text{H}_2\text{O})\}_2]$ neutral, centrosymmetric species and three water molecules of hydration (Figure 1).

All compounds share the $[\text{GeW}_{12}\text{O}_{40}]^{4-}$ cluster as the inorganic building block. This polyanion shows the characteristic structure of the α -Keggin isomer consisting of a central GeO_4 tetrahedron surrounded by 12 WO_6 octahedra arranged in four edge-shared W_3O_{13} trimers. The trimers are linked together and with the GeO_4 tetrahedron via corner-sharing. Bond lengths compared to those of the DFT-optimized Keggin anion²⁰ are listed in Table S1 in the Supporting Information.

{Cu(bpmen)} and {Cu(bpmpn)} Complexes. There are two types of Cu^{II}/N₂Py₂ complexes in the structures of **1** and **3** (N₂Py₂: bpmen and bpmpn, respectively). One of the complexes constitutes a metal–organic block supported on the Keggin anion (Cu1A), and the other one is a nonsupported $[\text{Cu}(\text{N}_2\text{Py}_2)(\text{H}_2\text{O})]^{2+}$ complex acting as a charge compensating unit (Cu1B). In both cases, the coordination spheres of all

copper(II) centers adopt tetragonally elongated CuN_4O square-pyramidal geometries, where the four N atoms of the ligand form the basal plane and the apical position is occupied by one terminal O atom from the cluster for Cu1A or one water molecule for Cu1B (Figure 2). In contrast, compound **2** contains only one type of Cu^{II}/bpmpn complex, which is grafted at the POM and whose Cu atom shows JT-elongated CuN_4OO octahedral geometry with four N atoms in the equatorial plane and one water molecule and one terminal O atom of the Keggin anion in axial positions. Bond lengths and angles of the metal–organic fragments in **1**–**3** (Table 2) are consistent with the few Cu^{II}/bpmen and Cu^{II}/bpmpn complexes reported to date.^{5,21}

Transition-metal complexes of bpmen and bpmpn can adopt two different geometrical isomers depending on the ligand conformation, and more specifically, on whether the N-methyl groups point to the same side of the CuN_4 plane (*cis*) or to opposite directions (*trans*).^{21d} In the case of copper(II), DFT-calculations have shown that the most favorable coordination geometries are square-pyramidal with *cis*-conformation for bpmen and octahedral with *trans*-conformation for bpmpn. This is exactly what we observe for **1** and **2**, but in contrast, the Cu^{II}/bpmpn complexes in **3** belong to the less favored *cis*-square pyramidal isomeric form.

Because of the strain caused by the 5-5-5 chelate ring around the transition metal (TM) center in bpmen complexes (Figure S3 in the Supporting Information), the dihedral angle between the pyridinic rings results significantly affected by the ligand conformation. This can be clearly observed in Figure 3, where the $\text{N}_{\text{Py}}-\text{N}-\text{N}-\text{N}_{\text{Py}}$ torsion angle of **1**–**3** and all 50 compounds deposited in the Cambridge Structural Database²² that contain TM/N₂Py₂ complex fragments (including those silicotungstate derivatives in our previous work) is represented against the C···C distance between N-methyl groups for each N₂Py₂ ligand bpmen and bpmpn. The N₄ torsion angle correlates with the above dihedral angle, whereas the C_{Me}···C_{Me} distance is a distinct parameter of each conformation. As a result, the TM/bpmen complex fragments are clearly gathered together in two well-separated regions, in such a way that *cis*-isomers with C_{Me}···C_{Me} distances shorter than 4.5 Å display torsion angles below 30°, whereas angles above 100° are usually observed for *trans*-isomers with C_{Me}···C_{Me} distances around 5.0–5.2 Å. It must be pointed out that most of the TM/bpmen complexes in the literature crystallize as *trans* conformers, whereas the *cis*-group is essentially formed by complexes in this

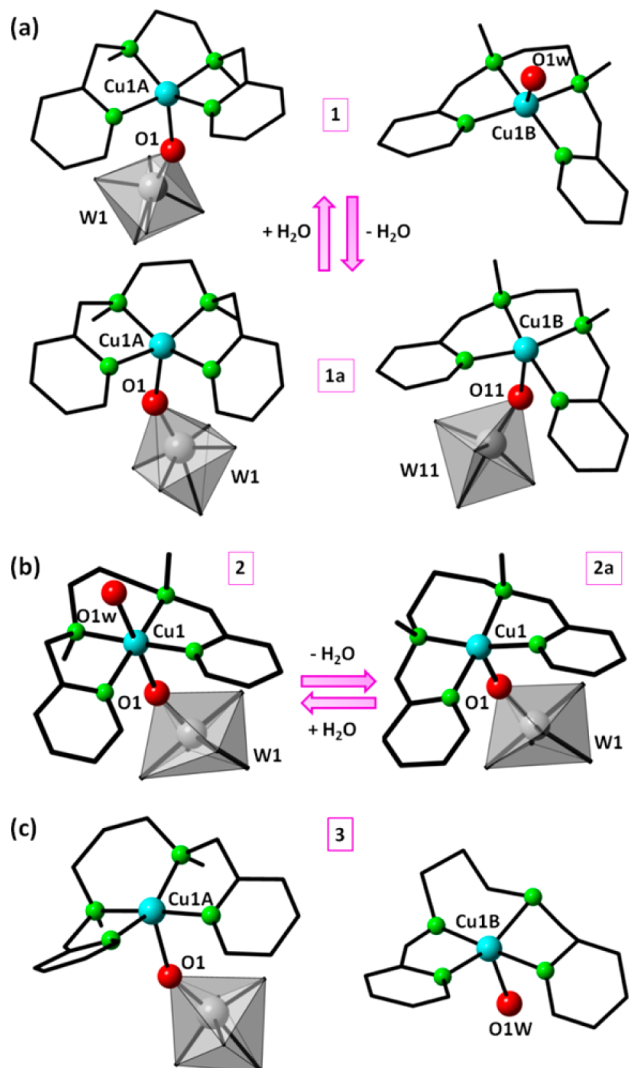


Figure 2. Representation of the $\text{Cu}^{\text{II}}/\text{N}_2\text{Py}_2$ complexes: (a) $\{\text{Cu}(\text{bpmen})\}$ metal–organic block and $[\text{Cu}(\text{bpmen})(\text{H}_2\text{O})]^{2+}$ cation in **1** compared to the corresponding fragments in the anhydrous **1a**. (b) $\{\text{Cu}(\text{bpmpn})(\text{H}_2\text{O})\}$ metal–organic block in **2** and its anhydrous form in **2a**. (c) $\{\text{Cu}(\text{bpmpn})\}$ metal–organic block and $[\text{Cu}(\text{bpmpn})(\text{H}_2\text{O})]^{2+}$ cation in **3**.

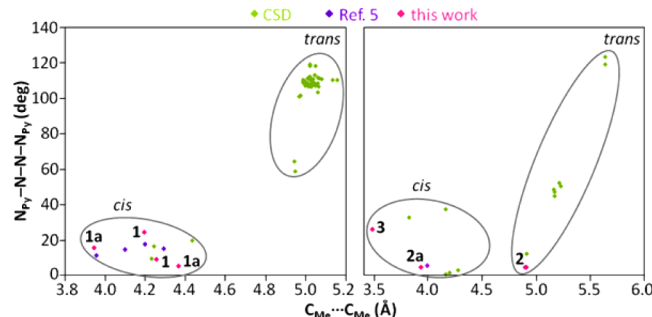


Figure 3. Representation of the $\text{N}_{\text{Py}}-\text{N}-\text{N}-\text{N}_{\text{Py}}$ torsion angle vs. the $\text{C}_{\text{Me}} \cdots \text{C}_{\text{Me}}$ distance for the $\text{Cu}^{\text{II}}/\text{N}_2\text{Py}_2$ fragments in this work, together with all TM/ N_2Py_2 complexes deposited in the CSD database. N_2Py_2 : bpmen (left), bpmpn (right).

and our previous work. This pattern is also reproduced in the case of TM/bpmpn complexes but with notably higher scattering, resulting in a worse defined *trans*-region as a result of the higher flexibility of the bpmpn ligand compared to bpmen. This higher flexibility originates from the additional methylene unit in the $\text{N}-(\text{CH}_2)_n-\text{N}$ bridge, which generates a S-6-S chelate ring around the metal center that minimizes the ring strain. In our case, the N_4 torsion angles are comparable for both **2** and **3** containing *trans* and *cis* $\text{Cu}^{\text{II}}/\text{bpmpn}$ isomeric forms, respectively.

Crystal Packing of 1. In close analogy to our previous $[\text{Cu}(\text{bpmen})(\text{H}_2\text{O})][\text{SiW}_{12}\text{O}_{40}\{\text{Cu}(\text{bpmen})\}]$ compound,⁵ the crystal packing of **1** also shows strong two-dimensional character with rows of monodecorated $[\text{GeW}_{12}\text{O}_{40}\{\text{Cu}(\text{bpmen})\}]^{2-}$ POMs along the [010] direction that are arranged in hybrid layers stacked along the crystallographic a axis (Figure 4). The pattern of POM–aromatic interactions between adjacent clusters in a row is similar to that observed in the Si-derivative, in such a way that one pyridinic ring of the grafted complex is sandwiched between contiguous $\{\text{W}_4\text{O}_{18}\}$ tetramers, while the second ring is placed over a $\{\text{W}_3\text{O}_{13}\}$ trimer of the adjacent cluster (Figure S4 in the Supporting Information). The distances of the ring centroids to the average planes of the trimers/tetramers defined by the O atoms are comparable to those reported for related POM-based hybrids.^{5,23}

However, the need to accommodate additional water molecules in the hemiheptahydrated phase of **1** results in a

Table 2. Selected Bond Lengths (\AA) for the $\text{Cu}^{\text{II}}/\text{bpmen}$ and $\text{Cu}^{\text{II}}/\text{bpmpn}$ Complexes in Compounds **1**, **2**, and **3** and the Anhydrous Phases **1a** and **2a**

$\text{Cu}^{\text{II}}/\text{bpmen}$ complexes		$\text{Cu}^{\text{II}}/\text{bpmpn}$ complexes				
	1	1a	2	2a		
Cu1A–N1A	2.024(12)	2.086(10)	Cu1–N1	2.010(10)	Cu1A–N1A	2.027(13)
Cu1A–N2A	2.052(13)	2.07(2)	Cu1–N2	2.032(11)	Cu1A–N2A	2.014(17)
Cu1A–N3A	2.006(12)	2.012(16)	Cu1–N3	2.014(10)	Cu1A–N3A	2.027(12)
Cu1A–N4A	1.980(11)	1.938(8)	Cu1–N4	1.978(10)	Cu1A–N4A	1.964(13)
Cu1A–O1	2.207(9)	2.195(11)	Cu1–O1A/O1B	2.49(2)/2.76(2)	Cu1A–O1	2.241(12)
			Cu1–O1w	2.748(13)		
Cu1B–N1B	2.017(11)	1.975(9)			Cu1B–N1B	2.08(3)
Cu1B–N2B	2.022(14)	2.011(15)			Cu1B–N2B	1.94(5)
Cu1B–N3B	2.034(11)	1.985(12)			Cu1B–N3B	2.02(7)
Cu1B–N4B	2.011(11)	1.977(13)			Cu1B–N4B	2.06(3)
Cu1B–O1w	2.200(10)				Cu1B–O1w	2.33(5)
Cu1B···O7	3.036(9)	2.772(11)				

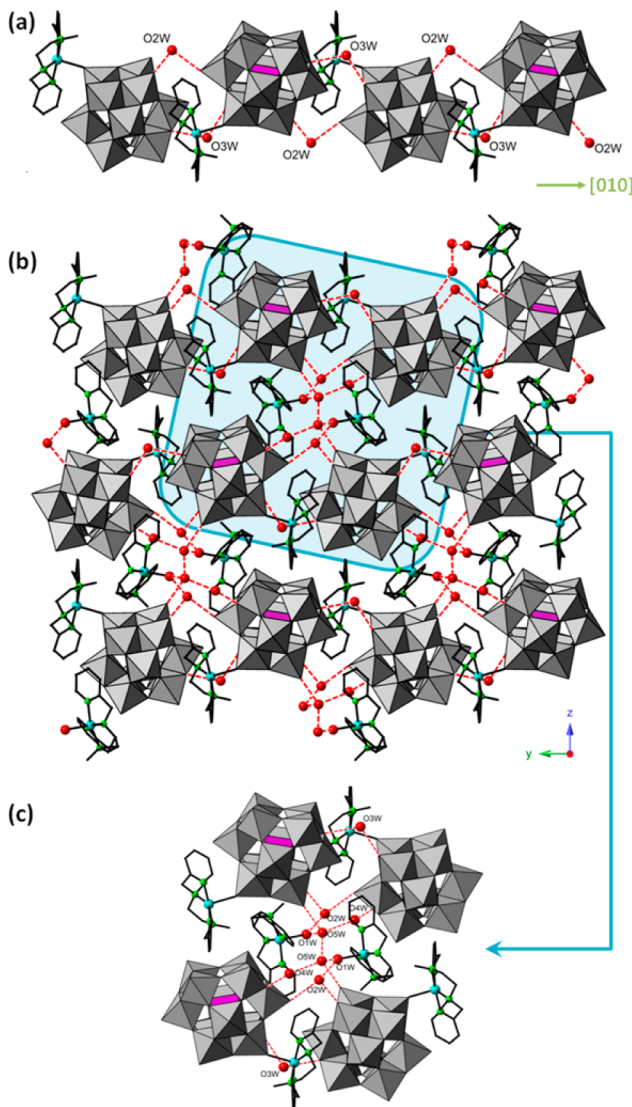


Figure 4. (a) Row of hybrid $[\text{GeW}_{12}\text{O}_{40}\{\text{Cu}(\text{bpmpn})\}]^{2-}$ POMs. (b) Crystal packing of **1** viewed along the a axis. (c) Detail of a cavity delimited by four hybrid POMs showing the hosted $[\text{Cu}(\text{bpmpn})(\text{H}_2\text{O})]^{2+}$ cations and hydration water molecules.

less compact crystal packing compared to that of the Si-derivative. This is clearly reflected in the Ge \cdots Ge distances between neighboring $[\text{GeW}_{12}\text{O}_{40}]^{4-}$ moieties in both the same row (13.1712(16) Å) and contiguous rows (13.5740(18) Å), which are significantly longer than those found in the nonhydrated phase containing $[\text{SiW}_{12}\text{O}_{40}]^{4-}$ species (11.890(5) and 11.934(5) Å). As a result of this larger separation between hybrid POMs, the intralamellar pockets occupied by the $[\text{Cu}(\text{bpmpn})(\text{H}_2\text{O})]^{2+}$ cations in the Si-derivative become open cavities in **1**. These cavities are delimited by four neighboring POMs and display room enough to host two complex cations and five water molecules of hydration each, which contribute to stabilize the crystal packing through an intricate network of strong hydrogen bonds involving terminal and bridging O_{POM} atoms and the aqua ligand of the complex cations (Table S2 in the Supporting Information). The enlargement of intralamellar spaces into cavities also modifies the pattern of reinforcing interactions established between the Keggin shells and the complex cations. The latter go from linking adjacent POMs in a row via

hydrogen bonds involving its aqua ligand to becoming stuck on the metal-oxo surface through interactions of the N1B and N4B rings with $\{\text{W}_3\text{O}_{13}\}$ and $\{\text{W}_4\text{O}_{18}\}$ fragments, respectively. Two water molecules of hydration ($\text{O}2\text{w}$, $\text{O}3\text{w}$) replace in turn the complex aqua ligands in the POM-connecting role.

Crystal Packing of 2. This compound is isostructural with our previous $[\text{SiW}_{12}\text{O}_{40}\{\text{Cu}(\text{bpmpn})(\text{H}_2\text{O})\}]_2 \cdot 3\text{H}_2\text{O}$ ⁵ and therefore, its crystal structure will be briefly discussed. It can be described as honeycomb-like metal-organic layers parallel to the (101) plane where the $\{\text{Cu}(\text{bpmpn})(\text{H}_2\text{O})\}$ fragments are connected through a complex network of C–H \cdots O_w and O_w–H \cdots O_w interactions involving methyl and pyridyl groups and coordination/hydration water molecules. Stacking of the metal-organic layers generates hexagonal channels running along the a axis where the Keggin clusters are hosted, in such a way that they occupy interlamellar spaces and result in being surrounded by six complexes from each adjacent metalorganic layer (Figure 5).

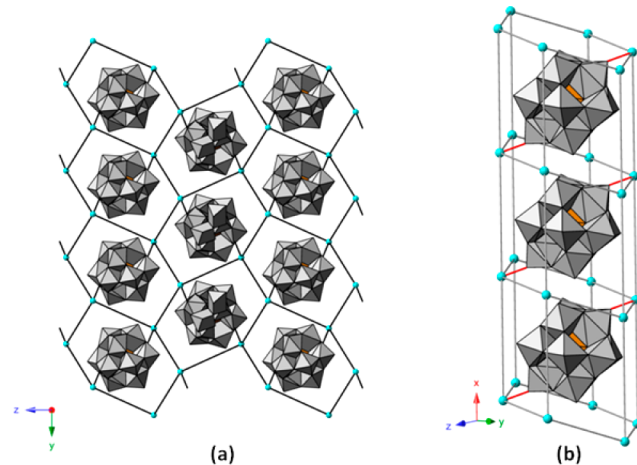


Figure 5. (a) Schematization of the honeycomb-like crystal packing of **2** viewed along the a axis (bpmpn ligands and water molecules are omitted for clarity). (b) Detail of a hexagonal channel parallel to the [100] direction with the Keggin POM guests.

Crystal Packing of 3. In spite of containing monodecorated $[\text{GeW}_{12}\text{O}_{40}\{\text{Cu}(\text{bpmpn})\}]^{2-}$ POMs and $[\text{Cu}(\text{bpmpn})(\text{H}_2\text{O})]^{2+}$ cations arranged in a two-dimensional lattice, significant differences can be found when comparing the structure of **3** to that of **1**. The crystal packing shows hybrid bilayers parallel to the ab crystallographic plane, which are formed by centrosymmetrically related hemilayers containing rows of monodecorated POMs along the [100] direction (Figure 6). Contiguous hybrid POMs in a row are held together by means of POM-aromatic interactions involving the pyridinic N1A ring of the supported complex, which is sandwiched between the tetrameric $\{\text{W}_4\text{O}_{18}\}$ faces of two adjacent Keggin clusters (Figure S5 in the Supporting Information). A massive network of C–H \cdots O_{POM} interactions is responsible for connecting neighboring POM rows in the hemilayers, as well as for linking the latter in the hybrid bilayers.

Stacking of the bilayers along the c axis is pillared by the $[\text{Cu}(\text{bpmpn})(\text{H}_2\text{O})]^{2+}$ cations, which arrange in such a way that the 1,3-diaminopropane bridge is inserted in the clefts of the hemilayers and the pyridinic rings point to the interlamellar region. The crystallographic disorder described for these species in the Experimental Section most likely arises from

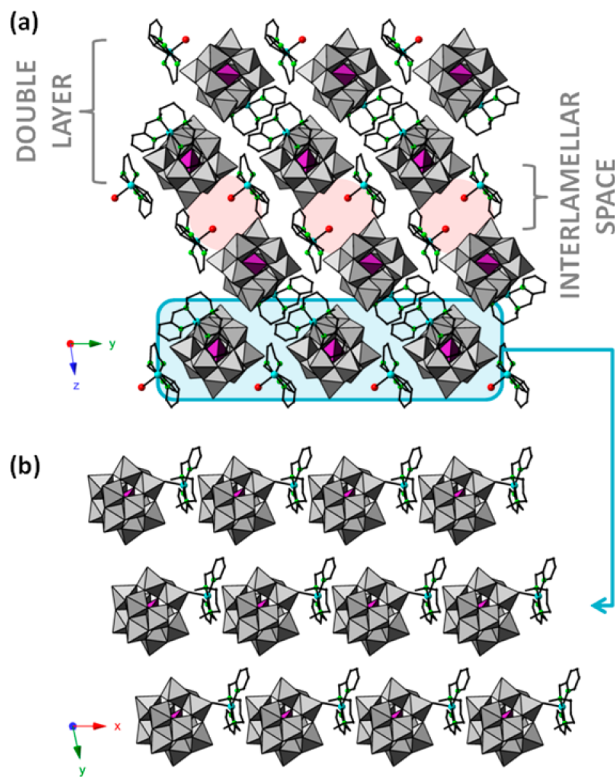


Figure 6. (a) Crystal packing of **3** viewed along the *a* axis (channels in the interlamellar region hosting the water molecules are highlighted in pink). (b) Detail of the double layer of hybrid [GeW₁₂O₄₀{Cu(bpmn)}]²⁺ POMs projected on the *ab* plane.

the fact that they are not involved in any significant network of intermolecular contacts. The complex cations acting as lamellar spacers generate rectangular hydrophilic channels parallel to the [100] direction with approximate dimensions of 5 × 6.5 Å. The apical aqua ligands are directed to the center of these channels, which most likely host all hydration water molecules. We could not determine the crystallographic positions for the latter due to disorder, but routine PLATON analyses reveal that the channels in the interlamellar region represent a solvent accessible void of 340 Å³ per unit cell. This empty volume is suitable to accommodate the eight water molecules determined from elemental analyses.

Thermo Structural Behavior. Thermal stability of compounds **1** and **2** was investigated by TGA/DTA. In the case of **3**, the fact that this compound is obtained only in trace amounts unfortunately prevented us from isolating enough crystalline material to perform reliable analyses. Thermal decomposition proceeded via three mass loss stages with almost identical profiles for **1** and **2** (insets in Figure 7). It starts at nearly room temperature with a mass loss stage (S1) of about 2% in both compounds. This stage originates from multiple overlapping endothermic processes and involves the release of all hydration/coordination water molecules (calcd for 4.5H₂O in **1**: 2.21, found: 2.25; calcd for 5H₂O in **2**: 2.43, found: 2.14). Dehydration is completed at ca. 100 °C for **1** and ca. 130 °C for **2**, and it leads to the anhydrous phases **1a** and **2a**, which show a wide range of thermal stability extending up to ca. 280 and 270 °C, respectively. The anhydrous phases undergo further decomposition via two highly overlapping mass loss stages of exothermic nature (S2 and S3) that must correspond to a combination of organic ligand combustion and

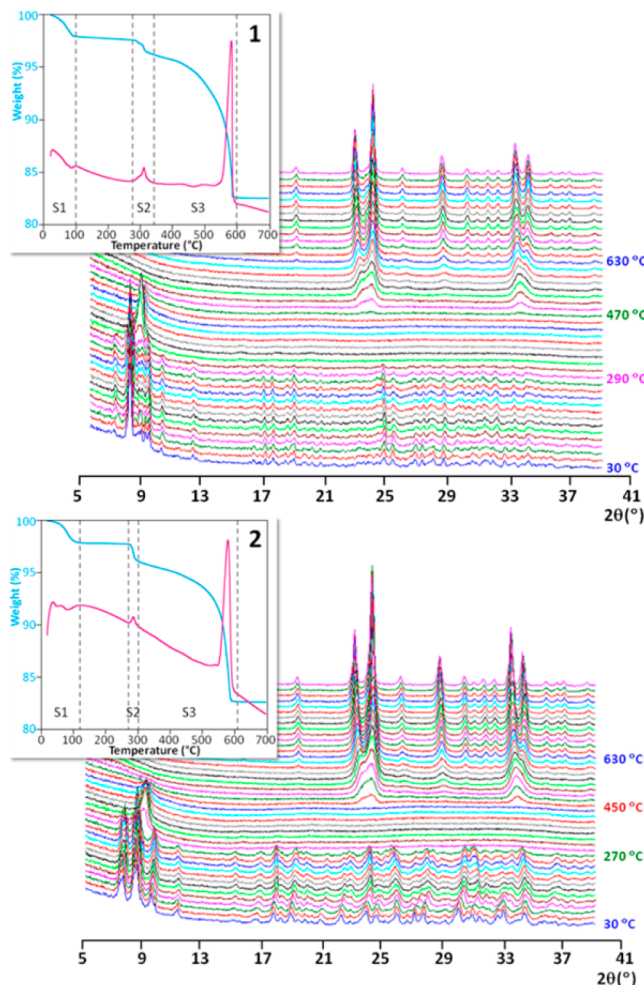


Figure 7. TGA/DTA curves (exo up) and variable temperature powder X-ray diffractograms of **1** (top) and **2** (bottom).

crumbling of the Keggin framework. The overall mass loss for these two stages is about 15% in both compounds, which is in good agreement with two N₂Py₂ ligands (calcd for 2C₁₆H₂₂N₄ in **1**: 14.74, found: 15.03; calcd for 2C₁₇H₂₄N₄ in **2**: 15.35, found: 15.04). The final residues are obtained above ca. 590 °C for **1** and 600 °C for **2** and have been identified by PXRD techniques as mixtures of monoclinic WO₃ (PDF 88269)²⁴ and triclinic CuWO₄ (PDF 431035)²⁵ with Scheelite-type structure (calcd for 2CuWO₄ + 10WO₃ + 1GeO₂: 83.04 in **1** and 82.21 in **2**, found: 82.60 and 82.71, respectively).

Comparison between the thermal behaviors of **2** and the Si-containing isostructural compound reveals that replacement of Si with Ge favors completion of the dehydration process but, in turn, confers higher thermal stability on the resulting anhydrous phase (145–255 °C for Si vs 130–270 °C for Ge). Simple TGA/DTA experiments were also performed to determine the reversibility of the dehydration processes. Crystalline samples of **1** and **2** were heated at a rate of 2 °C min⁻¹ up to 150 and 180 °C, and the so-generated anhydrous samples were kept for 1 day in an open container and then heated again at the same rate. The recorded TGA/DTA profiles are almost identical for both heating cycles (Figure S6 in the Supporting Information), showing that the anhydrous phases **1a** and **2a** are fully rehydrated to the original compounds **1** and **2** simply after some hours of exposure to room air.

Table 3. Unit Cell Parameters of **1** and **2** at Different Temperatures

T (°C)	lattice	a (Å)	b (Å)	c (Å)	α (deg)	β (deg)	γ (deg)	V (Å ³)
Compound 1								
-173	mP	11.5421(1)	22.4126(1)	25.8486(2)	90	102.422(1)	90	6529.7(1)
r.t.	mP	11.601(3)	22.629(4)	25.843(5)	90	103.72(4)	90	6591(3)
60	mP	11.590(4)	22.730(6)	25.567(15)	90	102.21(4)	90	6583(3)
105	mP	11.521(9)	22.570(15)	25.471(13)	90	103.12(5)	90	6450(7)
150	mP	11.4677(1)	22.5699(3)	25.3959(3)	90	102.372(1)	90	6420.4(2)
Compound 2								
-173	mP	11.0268(3)	12.1249(3)	24.7245(6)	90	96.305(2)	90	3285.6(1)
r.t.	mP	11.045(2)	12.186(4)	24.795(7)	90	96.40(3)	90	3317(2)
60	mP	11.036(3)	12.182(5)	24.82(2)	90	96.31(3)	90	3316.8(4)
105	mP	11.079(9)	12.140(13)	24.87(2)	90	96.71(7)	90	3322(4)
150	mP	10.9918(9)	12.0744(8)	24.242(2)	90	98.067(6)	90	3185.5(4)

PXRD experiments performed between room temperature and 890 °C show that crystallinity is retained up to 290 °C for **1** and 270 °C for **2** without substantial variations in the positions and intensities of the diffraction maxima (Figure 7). This indicates that both compounds undergo dehydration without collapse of the crystal packing and that formation of the anhydrous phases **1a** and **2a** does not result in alterations of the lattice type or in severe modifications of the unit cell parameters. The crystalline anhydrous phases undergo rapid amorphization at temperatures above ca. 300 °C, which is fully consistent with ligand combustion and Keggin crumbling stages taking place according to the above TGA analyses. New diffraction maxima belonging to the final residue appear at 450–470 °C and gain in intensity and definition up to 630 °C, where complete thermal decomposition is achieved as indicated by the TGA curves.

Analogous single-crystal XRD studies were also carried out to determine the structural changes promoted by the dehydration processes. Single crystals of **1** and **2** for which complete structural data were initially collected at 100(2) K were selected, and the temperature was raised from room temperature to 150 °C at a rate of 1 °C min⁻¹. Crystals of both compounds preserved their integrity and crystallinity in the complete temperature range, allowing for complete unit cell determinations at intervals of 45 °C (Table 3 and Figure S7 in the Supporting Information). In both cases, noticeable shortening of the *c* cell parameter with consequent decrease in the cell volume was observed when going from 105 to 150 °C. This range is in agreement with the temperatures at which **1a** and **2a** are formed according to TGA results. Therefore, the structures of the corresponding anhydrous phases could be determined from full data collections performed at 423(2) K. After the single crystals of the newly formed **1a** and **2a** were cooled to room temperature, they were kept under a wet atmosphere for a day, and intensity data were collected back at 100(2) K. The unit cells of the initial hydrated phases **1** and **2** were again obtained, and although collections were of poorer quality because of partial cracking during rehydration, crystals still diffracted acceptably enough for performing preliminary structural solutions. These observations demonstrate that dehydration of both **1** and **2** proceeds via SCSC transformations but furthermore that this process is fully reversible and the anhydrous **1a** and **2a** also undergo SCSC transformations promoted by consequent rehydration.

SCSC Transformation of **1 into **1a**.** Dehydration of **1** into **1a** proceeds through a SCSC transformation that has some features in common with the process described for the related

Si-containing phase. With the loss of the apical water molecule upon formation of **1a**, the complex cation Cu1B shifts toward the O_{POM} atom that was blocking its sixth position in **1** and preserves its square-pyramidal coordination geometry through grafting at the Keggin surface. Therefore, the anhydrous phase **1a** is configured by didecorated neutral species [GeW₁₂O₄₀{Cu(bpmen)}₂] where the metal–organic building blocks are supported on nonadjacent WO₆ octahedra belonging to two different {W₃O₁₃} trimers (Figure 8). The *cis* configuration of

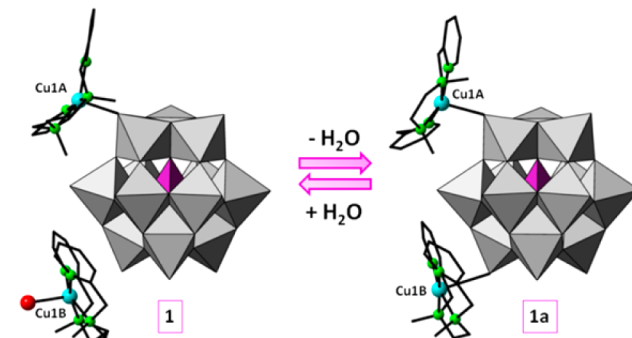


Figure 8. The monodecorated [GeW₁₂O₄₀{Cu(bpmen)}]²⁻ POM and the [Cu(bpmen)(H₂O)]²⁺ cation in **1** (left) compared to the didecorated [GeW₁₂O₄₀{Cu(bpmen)}₂] species in **1a** (right).

the bpmen ligand in the newly supported complex is maintained, but the change in the nature of the apical O atom causes a significant lengthening of ca. 0.55 Å in the corresponding Cu–O bond (Table 2). This bond and the N-methyl groups now point to different sides of the CuN₄ plane, preventing complex stabilization through intramolecular hydrogen bonding. The original Cu1A metal–organic block does not experience noticeable modifications when **1** is converted into **1a**.

Grafting of the complex cation on the POM surface upon dehydration was also observed for the Si-containing phase. However, the resulting [SiW₁₂O₄₀{Cu(bpmen)}₂] species is not isomorphic with **1a** but represents a different derivative because the two metal–organic blocks are supported on adjacent WO₆ octahedra belonging to the same {W₃O₁₃} trimer (Figure S8 in the Supporting Information). Making use of Pope and Scully's notation for metal-disubstituted α -Keggin clusters²⁶ and considering the WO₆ anchors as the positions where substitution takes places, the Keggin anion in **1a** would display metal–organic blocks grafted at relative $\alpha(1,5)$ positions, whereas the Si-containing didecorated species

would belong to the $\alpha(1,2)$ type. Formation of different geometrical isomers depending on the Keggin heteroatom is a direct consequence of the presence of hydration water molecules in **1**, which induce a relative arrangement of monodecorated POMs and complex cations different from that found in the nonhydrated phase containing Si-anions.

As a result of dehydration and consequent displacement of the Cu1B cations toward the POM rows, the structure of **1** shrinks in the [001] direction when it is transformed into **1a** (Figure 9). This compression is clearly reflected in the

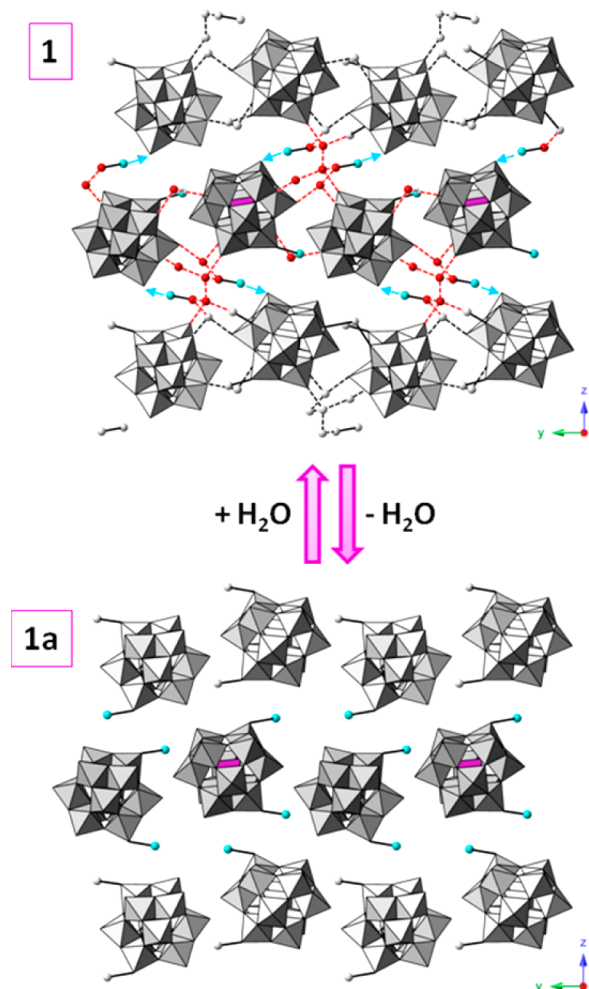


Figure 9. Comparison between the hybrid layers in **1** (top) and **1a** (bottom) highlighting the structural transformation promoted by the dehydration process in the colored central row (hydrogen bonds: dashed red lines; bpmen ligands omitted for clarity).

noticeable shortening of the *c* cell parameter (Table 3) and leads to a more compact stacking of the rows of newly generated didecorated clusters within the hybrid layers. In the absence of any O–H···O hydrogen bond, these rows are held together only by a complex network of C–H···O_{POM} contacts. In spite of the above compression, the intralamellar cavities are maintained when **1** is dehydrated into **1a**. The anhydrous phase shows an open-framework structure with slit-shaped micro pores of ca. $4.5 \times 6.5 \text{ \AA}$ dimensions that extend along the [100] direction (Figure S9 in the Supporting Information). Routine PLATON analyses reveal the presence in the unit cell of two solvent accessible voids of 164 \AA^3 each that are centered at $x, y, z = 0, 1/2, 0$ and $1/2, 1, 1/2$, respectively. For comparison,

similar analyses on the crystal packing of **1** upon removing the coordination/hydration water molecules from the structural data also results in two voids per unit cell centered at $x, y, z = 1/2, 1/2, 0$ and $1/2, 1, 1/2$ that account for 239 \AA^3 each. This evidences that the cavities undergo slight contraction but do not collapse when water molecules are released.

SCSC Transformation of **2 into **2a**.** In contrast to the bpmen system, the architecture of the didecorated cluster in **2** is maintained upon dehydration, resulting in the anhydrous form $[\text{GeW}_{12}\text{O}_{40}\{\text{Cu}(\text{bpmpn})\}_2]$ (Figure 10). However, the

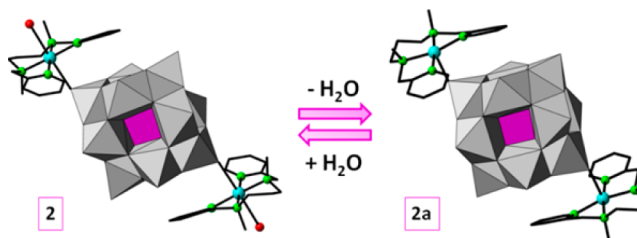


Figure 10. The didecorated $[\text{GeW}_{12}\text{O}_{40}\{\text{Cu}(\text{bpmpn})(\text{H}_2\text{O})\}_2]$ species in **2** (left) and its anhydrous form **2a** (right).

grafted complexes undergo some significant changes: release of the axial water molecule forces the coordination geometry around the Cu atoms to become square-pyramidal, and this process is accompanied by a *trans* to *cis* conformational change in the bpmpn ligand, which can only take place through rupture of the Cu–N bond involving one of the NCH₃ groups, followed by rotation of the latter and consequent recovery of the coordination (Figure S10 in the Supporting Information). Although the distances and angles related to the CuN₄ basal plane do not vary significantly, noticeable shortening of the Cu–O_{POM} distance is also observed.

Modifications in the crystal packing of **2** upon dehydration are relatively subtle but for an overall compression that is basically reflected in the shortening of the *c* cell parameter. The *trans* to *cis* ligand isomerization seems to play a key role in preserving the honeycomb pattern of the metal–organic layers by generating additional C–H···O_{POM} contacts that balance the loss of the C–H···O_w network (Table S2 in the Supporting Information). The overall contraction arises from a more compact packing of the Keggin clusters in the interlamellar space after release of interstitial water molecules of hydration, which in turn leads to the contraction of the metal–organic hexagonal motif around the clusters, as indicated by the shorter Cu···Cu distances compared to those found in **2** (Figure S11 in the Supporting Information). This process is analogous to that described for the isostructural Si-containing compound.

EPR Spectroscopy. The EPR Q-band spectrum of **1** is characteristic of magnetically isolated copper(II) chromophores with axial g tensor. The signal in the perpendicular region is centered at ca. 11800 G, and the parallel component shows a well-defined four-line hyperfine structure that originates from a spin doublet $S = 1/2$ interacting with a single $I = 3/2$ nucleus and spans in the range 10600–11300 G (Figure 11, left). The spacing between the four lines is not regular, and therefore, the signal cannot correspond to a single copper(II) center but rather to a combination of the individual contributions of the two crystallographically independent copper(II) atoms present in the structure of **1** with virtually identical coordination geometries (Cu1A and Cu1B). Best simulation of the spectrum is achieved by assigning the first and fourth lines on the parallel

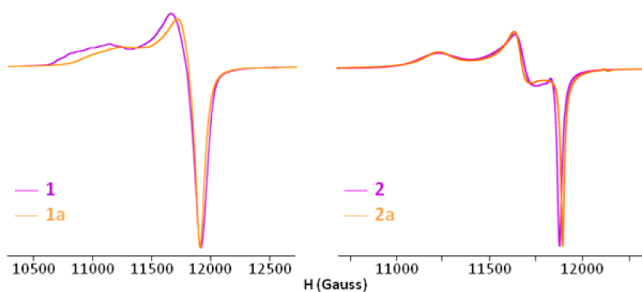


Figure 11. Comparison between the room-temperature Q-band EPR spectra of compounds **1/1a** (left) and **2/2a** (right).

region to different copper(II) centers and requires introduction of rhombic symmetry in \mathbf{g} and \mathbf{A} tensors. The resulting average values of the g_{\parallel} and A_{\parallel} components are reasonable for square-pyramidal chromophores with N_4 basal planes and apical elongation (Table S3 in the Supporting Information). Upon dehydration, the spectrum undergoes an upfield shift with consequent decrease of the g values and loss of resolution in the hyperfine structure of the parallel region. The former feature is characteristic of an increase in the apical elongation taking place, whereas the latter might indicate that this increase is not regular for both metallic centers. This is consistent with our structural data, which show that the apical Cu–O bond remains almost invariable for Cu1A when passing from **1** to **1a**, whereas significant lengthening of 0.55 Å is observed for Cu1B as a result of the change in the nature of the O atom (O_w to O_{POM}). Because of the above loss of resolution, the values of the A components have been kept constant for fitting the spectrum.

Although an analogous type of signal should be expected for **2** based on the structural similarities between its copper(II) complex moiety and those of **1**, the actual Q-band spectrum shows clear rhombic symmetry with no sign of hyperfine structure in the parallel region (Figure 11, right). Upon dehydration, the collapsed signal narrows and shifts to higher fields, but in contrast to what observed in the case of the transformation of **1** into **1a**, the g values calculated by simulation with rhombic symmetry do not undergo significant changes despite the fact that the octahedral CuN_4O_2 chromophore of **2** is converted into a square-pyramidal CuN_4O chromophore in **2a** with shortening of the apical Cu–O bond. Combination of these three features (rhombic symmetry, collapsed hyperfine structure, and invariable g components upon dehydration) indicates that the g tensors originating in the spectra of **2** and **2a** are of a cooperative nature rather than molecular tensors associated with the individual geometries of the copper(II) chromophores. Similar behavior was observed for the isostructural Si-containing compounds,⁵ and following our previous discussion, the spectra of **2** and **2a** could be attributed to exchange tensors ($G = 2.57$)²⁷ originating from long-range, extremely weak magnetic interactions taking place in our compounds.

CONCLUSIONS

This work represents a good indication that single-crystal to single-crystal (SCSC) transformations promoted by dehydration processes might be a common structural response to thermal stimulus in certain polyoxometalate-based inorganic–metalorganic hybrid compounds. We replaced Si^{IV} with Ge^{IV} in the hydrothermal reaction of Keggin-type precursors with Cu^{II} complexes of N_2Py_2 tetradeятate ligands and obtained the

compounds $[Cu(bpmen)(H_2O)][GeW_{12}O_{40}\{Cu(bpmen)\}] \cdot 3H_2O$ (**1**), $[GeW_{12}O_{40}\{Cu(bpmpn)(H_2O)\}] \cdot 3H_2O$ (**2**), and $[Cu(bpmpn)(H_2O)][GeW_{12}O_{40}\{Cu(bpmpn)\}] \cdot 8H_2O$ (**3**). Among the three compounds, only **2** is isostructural with the didecorated Si-containing cluster previously reported by us, whereas **1** and **3** containing monodecorated POMs and complex cations constitute new crystal phases.

Dehydration of both **1** and **2** leads to the thermally stable $[GeW_{12}O_{40}\{Cu(bpmen)\}_2]$ (**1a**) and $[GeW_{12}O_{40}\{Cu(bpmpn)\}_2]$ (**2a**) anhydrous phases, whose structures have been determined by single-crystal X-ray diffraction. Dehydrations are fully reversible upon exposure to air and proceed via SCSC transformations that imply rupture/formation processes in the copper(II) bonding and consequent geometrical and conformational modifications in the complex moieties. Thermally induced transformations in $[XW_{12}O_{40}]^{4-}/Cu(N_2Py_2)$ hybrid compounds appear to take place regardless of the size of the heteroatom X and the number of hydration water molecules present in the crystal packing. As observed for **2**, replacement of Si^{IV} with the larger Ge^{IV} does not affect the transformation pathway but confers larger thermal stability on the anhydrous phase. In contrast, structural rearrangement can be remarkably influenced by the presence of hydration water molecules in the phase precursor. In our case, heating the hemiheptahydrate phase **1** results in a didecorated cluster with the complex moieties grafted in a relative arrangement that differs significantly from that observed for the Si-derivative obtained from a nonhydrated precursor. Moreover, dehydration of **1** into **1a** does not result in a compact packing as for the Si-derivative but rather in an open-framework structure with slit-shaped micropores originating from the fact that the cavities hosting the water molecules do not collapse when the latter are released. To evaluate the factors that might facilitate this type of thermally induced crystal transitions in polyoxometalate hybrid compounds, we are planning to extend our studies to related systems containing other archetypical POM clusters or ligands with different characteristics regarding the denticity, rigidity vs flexibility, steric hindrance, or the capability to establish networks of weak intermolecular contacts.

ASSOCIATED CONTENT

S Supporting Information

IR spectra (Figure S1), PXRD diffractograms of **1**, **2**, and related precipitates (Figure S2); additional structural figures (Figures S3–S5, S8–S11); TGA/DTA profiles of the dehydration for **1** and **2** (Figure S6); thermal dependence of the unit cell parameters (Figure S7), additional structural tables (Tables S1 and S2); spin Hamiltonian parameters for **1/1a** and **2/2a** (Table S3). Crystallographic data in CIF format for **1**, **2**, **3**, **1a**, and **2a**. This material is available free of charge via the Internet at <http://pubs.acs.org>.

AUTHOR INFORMATION

Corresponding Author

*E-mail: juanma.zorrilla@ehu.es.

Notes

The authors declare no competing financial interest.

ACKNOWLEDGMENTS

This work has been funded by Eusko Jaurlaritza/Gobierno Vasco (EJ/GV) through the Program to Support the Research Groups of the Basque University System (Grant IT47710). The

authors thank Universidad del País Vasco UPV/EHU for financial support (Grant UFI11/53). A.I. and B.A. are indebted to EJ/GV for their predoctoral fellowships. Technical and human support provided by SGIKer (UPV/EHU) is gratefully acknowledged.

■ ABBREVIATIONS

bpmen, *N,N'*-dimethyl-*N,N'*-bis-(pyridine-2-ylmethyl)-1,2-diaminoethane; bpmpn, *N,N'*-dimethyl-*N,N'*-bis-(pyridine-2-ylmethyl)-1,3-diaminopropane

■ REFERENCES

- (1) (a) Pope, M. T. *Heteropoly and Isopoly Oxometalates*; Springer, Berlin, Germany, 1983. (b) Hill, C. L., Ed. *Chem. Rev.* **1998**, *98*, thematic issue 1. (c) *Polyoxometalates: From Platonic Solids to Anti-Retroviral Activity*; Pope, M. T., Müller, A., Eds.; Kluwer: Dordrecht, The Netherlands, 1994. (d) *Polyoxometalate Chemistry: From Topology via Self-Assembly to Applications*; Pope, M. T., Müller, A., Eds.; Kluwer: Dordrecht, The Netherlands, 2001. (e) *Polyoxometalate Chemistry for Nano-Composite Design*; Yamase, T., Pope, M. T., Eds.; Kluwer: New York, 2002. (f) Kortz, U., Ed. *Eur. J. Inorg. Chem.* **2009**, thematic issue 34. (g) Long, D.-L., Cronin, L., Guest Eds. *Dalton Trans.* **2012**, *33*, thematic issue 41. (h) Cronin, L., Müller, A., Guest Eds. *Chem. Soc. Rev.* **2012**, *41*, thematic issue 33. (i) Kortz, U., Liu, T., Guest Eds. *Eur. J. Inorg. Chem.* **2013**, thematic issue 10–11. (j) *Polyoxometalate Chemistry Some Recent Trends*; Sécheresse, F., Ed.; World Scientific: Singapore, 2013.
- (2) Dolbecq, A.; Dumas, E.; Mayer, C. R.; Mialane, P. *Chem. Rev.* **2010**, *110*, 6009.
- (3) (a) Gómez-Romero, P. *Adv. Mater.* **2001**, *13*, 163. (b) Long, D.-L.; Tsunashima, R.; Cronin, L. *Angew. Chem., Int. Ed.* **2010**, *49*, 1736.
- (4) See for example: (a) Chesnut, D. J.; Hagrman, D.; Zapf, P. J.; Hammond, R. P.; LaDuca, R., Jr.; Haushalter, R. C.; Zubietia, J. *Coord. Chem. Rev.* **1999**, *190*–*192*, 737. (b) San Felices, L.; Vitoria, P.; Gutiérrez-Zorrilla, J. M.; Reinoso, S.; Etxebarria, J.; Lezama, L. *Chem.—Eur. J.* **2004**, *10*, 5138. (c) Lisnard, L.; Dolbecq, A.; Mialane, P.; Marrot, J.; Codjovi, E.; Sécheresse, F. *Dalton Trans.* **2005**, 3913. (d) Reinoso, S.; Vitoria, P.; Gutiérrez-Zorrilla, J. M.; Lezama, L.; San Felices, L.; Beitia, J. I. *Inorg. Chem.* **2005**, *44*, 9731. (e) Jin, H.; Qi, Y.; Wang, E.; Li, Y.; Wang, X.; Qin, C.; Chang, S. *Cryst. Growth Des.* **2006**, *6*, 2693. (f) Reinoso, S.; Vitoria, P.; Gutiérrez-Zorrilla, J. M.; Lezama, L.; Madariaga, J. M.; San Felices, L.; Iturrospe, A. *Inorg. Chem.* **2007**, *46*, 4010. (g) Shi, D.-Y.; Zhao, J.-W.; Chen, L.-J.; Ma, P.-T.; Wang, J.-P.; Niu, J.-Y. *CrystEngComm* **2012**, *14*, 3108.
- (5) Iturrospe, A.; Artetxe, B.; Reinoso, S.; San Felices, L.; Vitoria, P.; Lezama, L.; Gutiérrez-Zorrilla, J. M. *Inorg. Chem.* **2013**, *52*, 3084.
- (6) (a) White, M. C.; Doyle, A. G.; Jacobsen, E. N. *J. Am. Chem. Soc.* **2001**, *123*, 7194. (b) Taktak, S.; Kryatov, S. V.; Haas, T. E.; Rybak-Akimova, E. V. *J. Mol. Catal. A* **2006**, *259*, 24. (c) Mas-Ballesté, R.; Costas, M.; Van den Berg, T.; Que, L. *Chem.—Eur. J.* **2006**, *12*, 7489. (d) Maklynets, O. V.; Rybak-Akimova, E. V. *Chem.—Eur. J.* **2010**, *16*, 13995. (e) Raffard, N.; Balland, V.; Simaan, J.; Létard, S.; Nierlich, M.; Miki, K.; Banse, F.; Anxolabéhère-Mallart, E.; Girerd, J. J. C. R. *Chimie* **2002**, *5*, 99. (f) Lyakin, O. Y.; Bryliakov, K. P.; Talsi, E. P. *Inorg. Chem.* **2011**, *50*, 5526. (g) Stránká, J.; Sebela, M.; Tarkowski, P.; Rehulk, P.; Chmelík, J.; Popa, I.; Pec, P. *Biochimie* **2007**, *89*, 135.
- (7) See for example: (a) Uchida, S.; Hashimoto, M.; Mizuno, N. *Angew. Chem., Int. Ed.* **2002**, *41*, 2814. (b) Ishii, Y.; Takenaka, Y.; Konishi, K. *Angew. Chem., Int. Ed.* **2004**, *43*, 2702. (c) Pang, H.; Zhang, Z.; Shi, D.; Chen, Y. *Cryst. Growth Des.* **2008**, *8*, 4476. (d) Ibrahim, M.; Dickman, M. H.; Suchopar, A.; Kortz, U. *Inorg. Chem.* **2009**, *48*, 1649. (e) Pang, H.; Peng, J.; Zhang, C.; Li, Y.; Zhang, P.; Ma, H.; Su, Z. *Chem. Commun.* **2010**, *46*, 5097. (f) Uchida, S.; Eguchi, R.; Nakamura, S.; Ogasawara, Y.; Kurosawa, N.; Mizuno, N. *Chem. Mater.* **2012**, *24*, 325. (g) Han, X.-B.; Zhang, Z.-M.; Wang, Z.-S.; Zhang, H.; Duan, H.; Wang, E.-B. *Inorg. Chem. Commun.* **2012**, *18*, 47. (h) Ogasawara, Y.; Uchida, S.; Maruichi, T.; Ishikawa, R.; Shibata, N.; Ikuhara, Y.; Mizuno, N. *Chem. Mater.* **2013**, *25*, 905.
- (8) See for example: Vittal, J. J. *Coord. Chem. Rev.* **2007**, *251*, 1781.
- (9) (a) Wéry, A. S. J.; Gutiérrez-Zorrilla, J. M.; Luque, A.; Ugalde, M.; Román, P. *Chem. Mater.* **1996**, *8*, 408. (b) Ritchie, C.; Streb, C.; Thiel, J.; Mitchell, S. G.; Miras, H. N.; Long, D.-L.; Boyd, T.; Peacock, R. D.; McGlone, T.; Cronin, L. *Angew. Chem., Int. Ed.* **2008**, *47*, 6881. (c) Zhang, L.-Z.; Gu, W.; Liu, X.; Dong, Z.; Li, B. *CrystEngComm* **2008**, *10*, 652. (d) Thiel, J.; Ritchie, C.; Streb, C.; Long, D.-L.; Cronin, L. *J. Am. Chem. Soc.* **2009**, *131*, 4180. (e) Uehara, K.; Mizuno, N. *J. Am. Chem. Soc.* **2011**, *133*, 1622. (f) Shi, L.-X.; Zhao, W.-F.; Xu, X.; Tang, J.; Wu, C.-D. *Inorg. Chem.* **2011**, *50*, 12387. (g) Uchida, S.; Takahashi, E.; Mizuno, N. *Inorg. Chem.* **2013**, *52*, 9320.
- (10) (a) Zhang, L.-Z.; Gu, W.; Dong, Z.; Liu, X.; Li, B. *CrystEngComm* **2008**, *10*, 1318. (b) Reinoso, S.; Dickman, M. H.; Praetorius, A.; Kortz, U. *Acta Crystallogr.* **2008**, *E64*, m614.
- (11) See for example: (a) Hu, Y.-Y.; Xiao, L.-N.; Wang, Y.; Zhao, D.-C.; Wang, L.-M.; Guo, H.-Y.; Cui, X.-B.; Xu, J.-Q. *Polyhedron* **2013**, *56*, 152. (b) Wu, Q.; Yang, H.; Cheng, H.-W.; Liu, Z.-G.; You, W.-S.; Gao, S. *J. Mol. Struct.* **2012**, *1030*, 83. (c) Wu, X.-Y.; Zhang, Q.-K.; Kuang, X.-F.; Yang, W.-B.; Yua, R.-M.; Lu, C.-Z. *Dalton. Trans.* **2012**, *41*, 11783.
- (12) (a) Pope, M. T.; Varga, G. M., Jr. *Inorg. Chem.* **1966**, *5*, 1249. (b) Pope, M. T.; Papaconstantinou, E. *Inorg. Chem.* **1967**, *6*, 1147. (c) Papaconstantinou, E.; Pope, M. T. *Inorg. Chem.* **1967**, *6*, 152. (d) Maestre, J. M.; López, X.; Bo, C.; Casañ-Pastor, N. *J. Am. Chem. Soc.* **2001**, *123*, 9571. (e) Poblet, J. M.; López, X.; Bo, C. *Chem. Soc. Rev.* **2003**, *32*, 297. (f) Mbomekallé, I.-M.; López, X.; Poblet, J. M.; Sécheresse, F.; Keita, B.; Nadjo, L. *Inorg. Chem.* **2010**, *49*, 7001.
- (13) Tézé, A.; Hervé, G.; Finke, R. G.; Lyon, D. K. In *Inorganic Syntheses*; Ginsberg, A. P., Ed.; John Wiley & Sons: Hoboken, NJ, 1990; Vol. 27, pp 85–96.
- (14) *CrysAlisPro Software System*; Agilent Technologies UK Ltd.: Oxford, UK, 2012.
- (15) Dolomanov, O. V.; Bourhis, L. J.; Gildea, R. J.; Howard, J. A. K.; Puschmann, H. *J. Appl. Crystallogr.* **2009**, *42*, 339.
- (16) Sheldrick, G. M. *Acta Crystallogr.* **2008**, *A64*, 112.
- (17) Macrae, C. F.; Bruno, I. J.; Chisholm, J. A.; Edgington, P. R.; McCabe, P.; Pidcock, E.; Rodriguez-Monge, L.; Taylor, R.; van de Streek, J.; Wood, P. A. *J. Appl. Crystallogr.* **2008**, *41*, 466.
- (18) Spek, A. L. *Acta Crystallogr.* **2009**, *D65*, 148.
- (19) Farrugia, L. J. *J. Appl. Crystallogr.* **1999**, *32*, 837.
- (20) San Felices, L.; Vitoria, P.; Gutiérrez-Zorrilla, J. M.; Lezama, L.; Reinoso, S. *Inorg. Chem.* **2006**, *45*, 7748.
- (21) (a) Kani, Y.; Ohba, S.; Kunita, M.; Nishida, Y. *Acta Crystallogr.* **2000**, *C56*, e197. (b) Mautner, F. A.; Mikuriya, M.; Ishida, H.; Sakiyama, H.; Louka, F. R.; Humphrey, J. W.; Massoud, S. S. *Inorg. Chim. Acta* **2009**, *362*, 4073. (c) Glerup, J.; Goodson, P. A.; Hoddyson, D. J.; Michelson, K. *Inorg. Chem.* **1995**, *34*, 6255. (d) Pandiyan, T.; Guadalupe, H. J.; Cruz, J.; Bernès, S.; Ugalde-Saldivar, V. M.; González, I. *Eur. J. Inorg. Chem.* **2008**, 3274. (e) Xu, H.; Sato, O.; Li, Z.; Ma, J. *Inorg. Chem. Commun.* **2012**, *15*, 311. (f) Yokoyama, T.; Yoshise, M.; Hase, S.; Kawate, A.; Akashi, H.; Zenki, M. *X-ray Struct. Anal. Online* **2011**, *27*, 51.
- (22) Allen, F. H. *Acta Crystallogr.* **2002**, *B58*, 380.
- (23) (a) Reinoso, S.; Vitoria, P.; San Felices, L.; Lezama, L.; Gutiérrez-Zorrilla, J. M. *Inorg. Chem.* **2006**, *45*, 108. (b) Ugalde, M.; Gutiérrez-Zorrilla, J. M.; Vitoria, P.; Luque, A.; Wéry, A. S. J.; Román, P. *Chem. Mater.* **1997**, *9*, 2869.
- (24) Schofield, P. F.; Knight, K. S.; Redfern, S. A. T.; Cressey, G. *Acta Crystallogr.* **1997**, *B53*, 102.
- (25) Woodward, P. M.; Sleight, A. W.; Vogt, T. *J. Phys. Chem. Solids* **1995**, *56*, 1305.
- (26) Pope, M. T.; Scully, T. F. *Inorg. Chem.* **1975**, *14*, 953.
- (27) Hathaway, B. J.; Billing, D. *Coord. Chem. Rev.* **1970**, *5*, 143.